17. Fracture Toughness of Cemented Carbides

J.L. Chermant and F. Osterstock
Equipe Materiaux. Microstructure
Laboratoire de Cristallographie et Chimie du Solide L.A. 251
I.S.M.R.A. - Université
14032 CAEN Cedex - France

Summary

Fracture toughness parameters have been determined for a large number of different tungsten carbide-cobalt alloys. SENB specimens with spark eroded notches were used. The use of DCB specimens enabled us to assess the SENB results and to obtain K_I, V diagrams. These diagrams show that the same mechanisms act at low and high crack propagation rates. Two mechanisms act simultaneously. The relative contribution to the strain energy release rate depends on the size of a zone in which the various processes can take place. The nature of these processes and the width of this zone need further experimental investigation.

Introduction

Fracture toughness measurements on cemented tungsten carbide - cobalt alloys have been carried out for many years. Many of the results obtained are in agreement (1) (2) (3) (4) (5). Several models of crack propagation have been proposed, based either on crack opening displacement criteria (3) (5) or on dislocation pile-up mechanisms (1) (4) or simply on surface energies (6) (7). One of the most commonly used criteria to decide upon the fracture mechanism is the nature of the fracture surface: mainly intergranular decohesion of carbide crystalsand tearing of the cobalt layers or mainly transgranular fracture of the carbide crystals.Moreover a very strong dependence of the fracture toughness parameters on the microstructural parameters is observed. However, if an attempt is made to equate these parameters to those in the crack propagation models (3)(5) different results are obtained.

The aim of this work is to present the results which were obtained on tungsten carbide-cobalt alloys series covering a wide range of mean diameters of the carbide crystals(0.7 /um to 6.5 /um) and of volume fractions of cobalt (5 to 37 %). The fracture toughness parameters obtained with these specimens are

correlated with the microstructural parameters for the alloys.
It should thus be possible to obtain qualitative information on the deformation and fracture processes occuring at the crack tip as it advances.

Experimental details

The alloys used are divided in five series having mean diameters of carbide crystals of 0.7, 1.1, 2.2, 5.0 and 6.5 /um. The three first series had volume fractions of cobalt of 5, 10, 15, 22, 30 and 37 % and were sintered by the Ugine Carbone Company. The 5.0 /um diameter series was available with cobalt volume fractions of 5, 10 and 15 % and the 6.5 /um series with cobalt volume fractions of 30 and 37 %. Both the 5.0 /um and 6.5 /um diameter series were obtained in the laboratory by inducing crystal growth in the series with a mean diameter of the carbide crystals of 2.2 /um at 1450°C in argon. Specimens of pure carbide ($\bar{D}_{WC}$ = 6.5 /um) and bounded with 0.5 % cobalt in volume ($\bar{D}_{WC}$ = 6.5 /um) were also tested.
All these series were tested using the SENB method in three point bending. The knife edge supports were 32 mm apart. The notches were produced by spark erosion cutting. The cutting tool was a thin copper foil between 20 and 25 /um thick. Further details can be found in the literature (8).
In order to assess the SENB results, DCB measurements were carried out on the series with a mean diameter of carbide crystals of 2.2 /um. The specimens were 3 x 30 x 80 mm^3. A slot, 1 mm deep, was made on one side of the specimen in order to keep the notch in the center of the specimen. A natural sharp notch was obtained by inducing sub-critical crack growth in a spark eroded notch.

Results

1) Influence of the cobalt content.
The influence of the cobalt content on the critical stress intensity factor, K_{1C}, is shown in figure 1. K_{1C} increases with the volume fraction of cobalt for each mean diameter of the carbide crystals and also with the mean diameter of the carbide crystals at a fixed cobalt volume fraction. The K_{1C} values range from 9 MPa. $m^{1/2}$ to 23 MPa.$m^{1/2}$, and the extrapolation to zero cobalt volume fraction gives the same value of 8.8 MPa. $m^{1/2}$ for pure carbide in the range of mean diameters investigated.
Figure 2 shows the variation of mechanical properties in materials of composition ranging from pure carbide to 5 % cobalt in volume. The mechanical properties

measured were the rupture stress in bending, σ_{rf}, and in compression, σ_{rc}, and the critical stress intensity factor K_{1C}. In each case a rapid increase with increasing volume fraction of cobalt is observed. It demonstrates that an extrapolation to pure carbide values is invalid. This is particularly noticeably in the case of the fracture toughness parameter for which a K_{1C}-value of 7.5 MPa. $m^{1/2}$ is measured on pure WC instead of a K_{1C} value of 8.8 MPa. $m^{1/2}$ as obtained by extrapolation from the tungsten carbide-cobalt alloys. Furthermore a small amount of cobalt, i.e. 0.5 % in volume, a quantity just sufficient to produce a thin binder layer between the carbide crystals, causes a marked increase in the fracture toughness for pure carbide and attains the level obtained by extrapolation.

2) DCB measurements and K_1, V diagram.

Double Cantilever Beam specimens with a natural sharp notch were also tested in order to assess the results obtained with the Single Edge Notched Bending specimens where the notches were only spark eroded.

Figure 3 shows the experimental arrangement used to make these measurements. A spark eroded notch was first introduced into the specimen and then sub-critical crack-growth was induced to produce a natural sharp notch. A clip gauge was used to measure the displacement of the loading points. The specimen was loaded to just below the critical fracture load, the crosshead was then stopped and the relaxation of the load was recorded. The load-displacement curves were recorded independently with a Hewlet-Packard 75001B flat-bed recorder.

K_1-crack velocity diagrams were then evaluated according to the method proposed by A.V. VIRKAR and R.S. GORDON (9). The value of the stress intensity factor is given by:

$$K_1 = \frac{3.46\ Fa\ \left[1 + 1.32\ (h/a) + 0.532\ (h/a)^2\right]^{1/2}}{(e\ b)^{1/2}\ h^{3/2}}$$

where:

F: applied load
a: crack length
h: half width of the specimen
b: thickness of the specimen
e: thickness of the specimen at the slot

The compliance of the specimen, C(a), is given by:

$$C(a) = \frac{24}{Ebh^3}\ (0.333\ a^3 + 0.66\ ha^2 + 0.542\ h^2a)$$

where E is the Young modulus of the alloy tested.

The compliance of the specimen can be calculated from the loading point displacement, $y = C(a) \cdot F$, and hence the value of the crack length, a, can be read off a diagram or it can be calculated using a computer program. The applied load, F, and the crack length yield the value of the stress intensity factor, K_1, at each instant.

The crack propagation velocity, V, is given by:

$$V = \left(C_M + \frac{24\ P(a)}{Ebh^3}\right) \frac{dF}{dt} \Big/ \frac{24\ P(a)}{Ebh^3} F$$

where:

C_M: compliance of the machine

$P(a) = (0.333\ a^3 + 0.66\ ha^2 + 0{,}542\ h^2a)$

$P(a) = (a^3 + 1.32\ ha + 0.542\ h^2)$

Figure 4 shows the K_1,V diagrams obtained using this method. The crack velocity is between 10^{-7} m/s and 10^{-2} m/s but difficulties were encountered when attempts were made to reach velocities higher than 10^{-3} m/s. Figure 4 shows a log V - log K_1 plot. No lower K_1-limit for crack propagation could be observed in the range of velocities studied.

In addition it is worth pointing out that at these velocities crack growth occurs within 10 % of the K_{1C} value, i.e. the crack propagates sub-critically between 0.90 K_{1C} and K_{1C}. K_1 and V are related by the expression $V = AK_1^n$ where the experimental value of n lies between 140 and 180. However no precise correlation between n and the microstructural parameters was observed. Furthermore electron microscope observations of the fracture surfaces revealed no differences in the fracture patterns at low and high crack velocities thus confirming an observation made earlier by M.J. MURRAY and C.M. PERROT (10) on Double Torsion specimens. It was therefore concluded that the same fracture mechanism is operating at low and high crack-velocities.

Due to the strong influence of K_1 on the crack velocity and to the narrow range of subcritical crack growth, a velocity of $V = 10^{-3}$ m/s was considered to be critical for SENB specimens. Figure 5 provides comparison between the SENB and the DCB results. The K_{1C}-values obtained with spark erosion notched SENB

specimens and the K_1-value corresponding to a crack velocity of 10^{-3} m/s obtained with the natural notched DCB specimens are both plotted. Both parameters vary in a likeway with increasing cobalt content and in addition the K_1-values obtained with the two methods agree within some percent. The only K_1-value not agreeing is the one for a volume fraction of cobalt of 10 %. This is a weakness of the SENB specimens with spark eroded notches where one is always dependent on the quality and the shape of the sharp notch.

3) Dependence on microstructural parameters

The SENB-results were used to investigate the fracture mechanisms in these alloys by using the dependence of the fracture toughness on microstructural parameters. The most important microstructural parameters are the mean diameter of the carbide crystals, $\bar{D}_{WC}$, the contiguity of the carbide phase, C_{WC}, and the mean free path in the cobalt phase, $\bar{L}_{Co}$.

Figure 6 shows the dependence of the critical stress intensity factor, K_{1C}, on the contiguity of the carbide phase, C_{WC}. K_{1C} decreases with increasing contiguity, i.e. the more possibilities presented to the crack to follow a carbide-carbide boundary. Contiguity is defined as the ratio of the contact surface over the total surface of the carbide crystals and may thus be related to physical phenomena like interfacial carbide-carbide decohesion or energy consuming sliding of the interfaces.

Toughness is also dependent on the cobalt phase and figure 7 shows the variation of the strain energy release rate, G_{1C}, with the microstructural parameter $\bar{L}_{Co}{}^2/\bar{D}_{WC}$. This parameter is obtained by equating the energy of a dislocations pile-up in the cobalt to the energy necessary to break a carbide crystal (4). Two linear variations are obtained, but are not an indication of two different fracture mechanisms. They are due either to the fact that the larger grain sizes were obtained by inducing crystal growth in the 2.2 /um-series and thus changing some what the composition of the cobalt phase, or to the presence of very large carbide crystals which are fractured more than once hence consuming more energy (see Fig. 12).

4) Processes at the crack tip

Most of the fracture energy, the strain energy release rate, G_{1C} is dissipated at the crack tip in the form of plastic deformation. The question still remains unanswered, whether only the cobalt phase or both the cobalt and the carbide phases deform plastically.

A general observation is that fracture changes from almost complete intergranular decohesion of the carbide crystals at low volume fractions of cobalt (Fig. 8) to almost complete transgranular fracture of the carbide crystals at high cobalt volume fractions (Fig. 9). Furthermore it is sometimes believed that a carbide crystal diameter of $\sim$2 /um is a critical value above which transgranular fracture of the carbide crystals occurs. Intergranular decohesion of the carbide-carbide interfaces and tearing of the cobalt phase take place at lower grain sizes. However, the correlations obtained do not show that different mechanisms are acting at low and high volume fractions of cobalt or for small and large diameters of the carbide crystals.

In an earlier work (4) (8) some quantitative results were obtained on the proportions of the different types of fracture. The measurements were made on the fracture path, i.e. the intersection of the fracture surface and the side of the specimen, of polished and etched K_{1C} specimens which were not completely fractured. Thus the two faces of the fracture remain in contact with each other and it could be decided if fracture occured by cleavage of the carbide crystals or interfacial decohesion of carbide crystals or cobalt-carbide debonding. The general tendence was a change from 70 % to 35 % interfacial decohesion of the carbide crystals when the cobalt volume fraction increased from 5 % to 37 %. The percentage with respect to the total crack length counted of cleaved carbide crystals passed through a maximum at approximatively 15 % cobalt in volume. Hence the percentage of cleaved carbide crystals with respect to the carbide phase increased. These measurements were made on specimens having a mean diameter of the carbide crystals of 2.2 /um.

The processes occuring at the crack tip are different in nature.

- cleavage fracture of the carbide crystals,
- sliding and interfacial decohesion of the carbide-carbide boundaries,
- cobalt-carbide decohesion,
- and deformation and tearing of the cobalt phase.

It is likely that two principal mechanisms are acting simultaneously:

- sliding and interfacial decohesion of the carbide-carbide boundaries.
- deformation of the cobalt phase and cleavage of the carbide crystals.

The relative importance of each mechanism depends on the size of a "process zone" by comparison with concepts used with ceramic materials (11),

rather than on the plastic zone radius. The concept of process zone should be used because of the inhomogene nature of WC-Co materials. This leads to a plastically deformed region ahead of the crack in which elastic "islands" i.e. the carbide crystals are present. Since the elastic constants of the carbide are much higher than that of the cobalt, the "plastic zone" can extent over several carbide crystals and the plastic deformation is limited to the cobalt phase.

Although the fact that tungsten-carbide cobalt alloys are plastically non-homogeneous materials we have calculated values of plastic zone radius with macroscopic yield stress values corresponding respectively to 0.05 % and 0.5 % plastic strain. The values obtained are plotted as a function of the mean free path in the cobalt phase as shown in figure 10. It can be observed that a unique relationship exists between the two parameters and that at the lower values the radius is of the same order of magnitude as the mean free path in the cobalt phase, i.e. much less than one crystal diameter. For the larger values it increases rapidly, becoming several times larger than the mean diameter of the carbide crystals. On the other hand the plastic zone radius seems to play an important role in the crack propagation processes as can be seen in figure 11 where a linear relationship exists between the strain energy release rate. G_{1C}, and the square root of the plastic zone radius.

Conclusion

It would seem that two mechanisms are simultaneously operative in the crack propagation. To decide on the relative importance of each it is necessary to introduce the concept of process zone rather than the size of the plastic zone only. Further work is necessary in order to obtain more information on the process zone size and the processes occuring in it (Figure 12)

Aknowledgements: This work was supported by the Délégation Générale á la Recherche Scientifique et Technique, Contract No 76.7.0613.

References

1. R.C. Lueth, Ph.D. Thesis, Michigan State Univ. 1972.
2. S.S. Yen, M.S. Thesis, Lehigh Univ., 1971.
3. J.R. Pickens and J. Gurland, Mat. Sci. Eng., 1978, 33, 135 - 142
4. J.L. Chermant and F. Osterstock, J. Mater. Sci., 1976, 11, 1939 - 1951.
5. M.J. Murray, Proc. Roy. Soc. Lond., 1977, A 356, 483 - 508.
6. T. Johannesson, 4th European Symposium for Powder Metallurgy, Grenoble, 13. - 15. May 1975.
7. H. Hübner, Z. Metallkunde, 1976, 67 (8), 507 - 513.
8. F. Osterstock, Dr.-Ing. Thesis, Université de Caen, 1975.
9. A.V. Virkar and R.S. Gordon, J. Am. Ceram. Soc., 1976, 59, 68.
10. M.J. Murray and C.M. Perrot, Proceedings of the 1976 Int. Conference on Hard Material Tool Technology, Carnegie Mellon Inst ., June 22 - 24, 1976.
11. F.E. Buresh, "Sience of Ceramics", 1973, 7, 473.

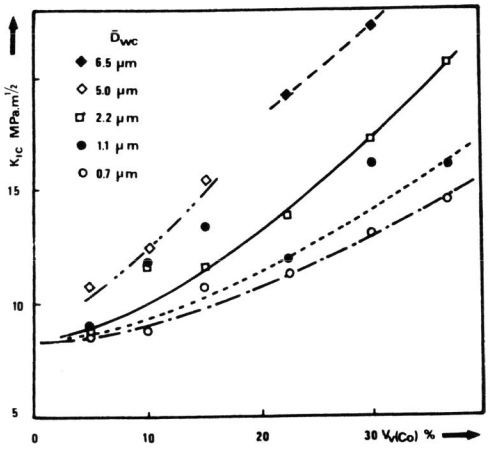

Fig. 1: Variation of K_{1C} with the volume fraction of cobalt

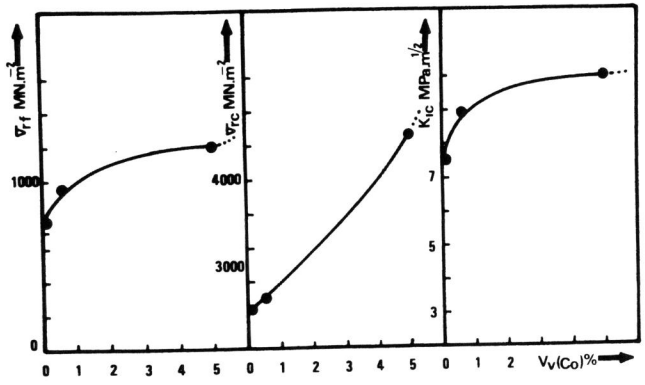

Fig. 2: Variation of mechanical properties at low cobalt volume fractions

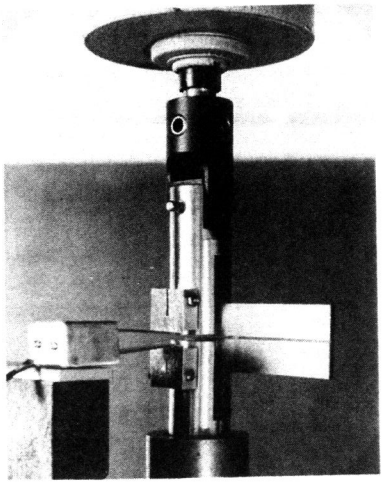

Fig. 3: Experimental arrangement for K_1, V measurements on DCB specimens

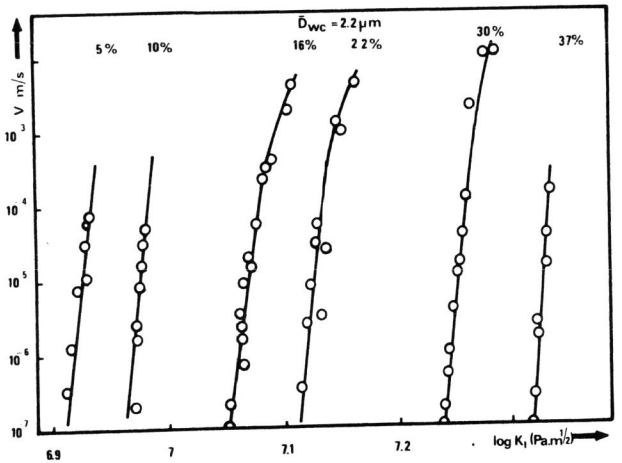

Fig. 4: K_1, V diagram as obtained from DCB specimen measurements

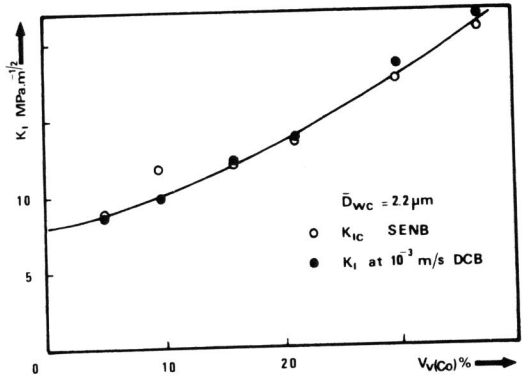

Fig. 5: Comparison of SENB and DCB results

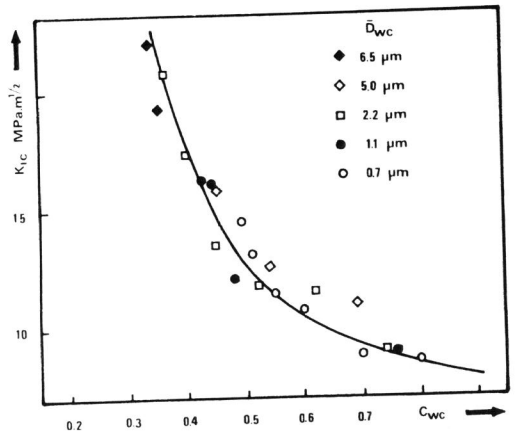

Fig. 6: Variation of K_{1C} with the contiguity of the carbide phase.

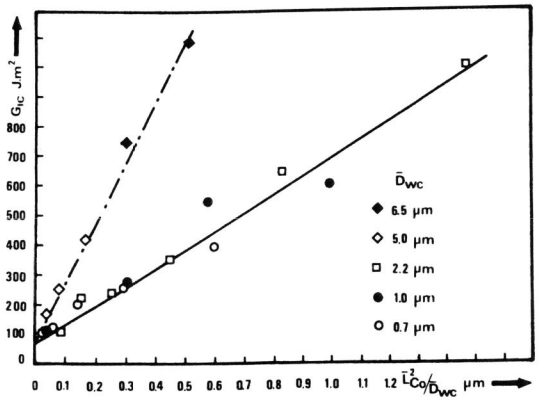

Fig. 7: Variation of G_{1C} with $\bar{L}_{Co}^{\ 2} / \bar{D}_{WC}$

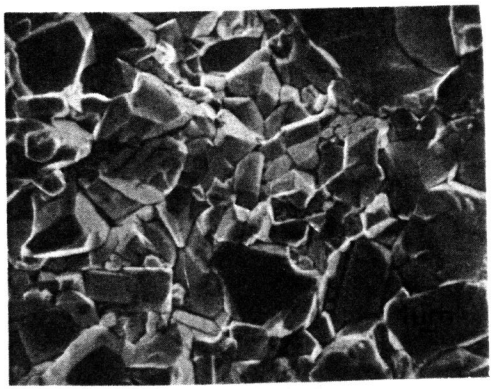

Fig. 8: Fractograph from a K_{1C} specimen ($\bar{D}_{WC}$ = 2.2 µm, Vv(Co) = 0.5 %)

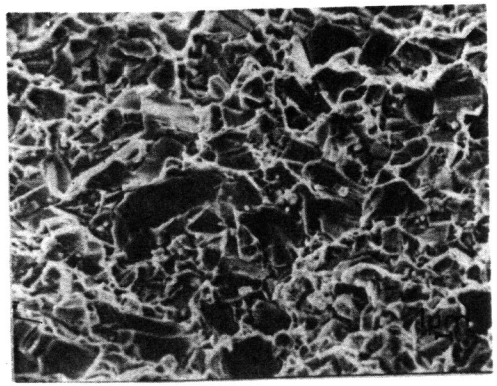

Fig. 9: Fractograph from a K_{1C} specimen ($\bar{D}_{WC}$ = 2.2 µm, Vv (Co) = 30 %)

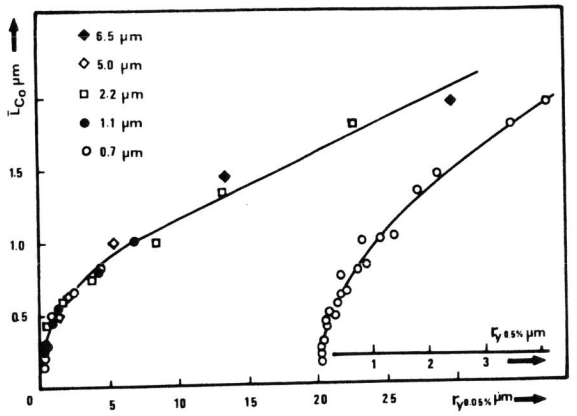

Fig. 10: Variation of plastic zone radius r_y, with $\bar{L}_{Co}$

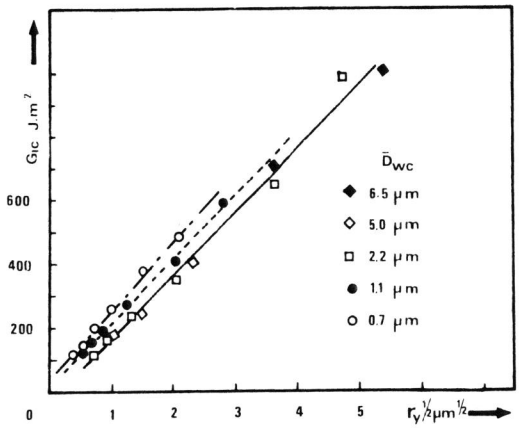

Fig. 11: Variation of G_{1C} with $r_y^{1/2}$

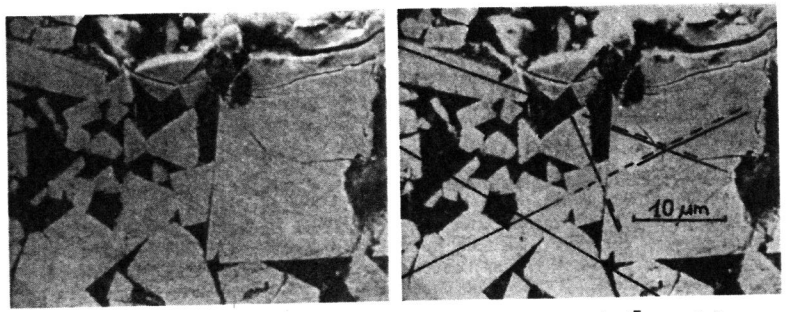

Fig. 12: Grain boundary sliding near the fracture path ($\bar{D}_{WC}$ = 6.5 µm, Vv (Co) = 30 %)